REPORT DOCUMENTATION PAGE

AFRL-SR-AR-TR-04-

0171

1. REPORT DATE (DD-MM-YYYY)	2. REPORT TYPE	3. DATES COVERED (From - To)
	Final Report	Sep 1, 02 - Aug 31, 03

4. TITLE AND SUBTITLE
On-Line Trajectory Optimization for Autonomous Air Vehicles

5a. CONTRACT NUMBER

5b. GRANT NUMBER
F49620-02-C-0085

5c. PROGRAM ELEMENT NUMBER

6. AUTHOR(S)
Dr. J. Eric Corban

5d. PROJECT NUMBER

5e. TASK NUMBER

5f. WORK UNIT NUMBER

7. PERFORMING ORGANIZATION NAME(S) AND ADDRESS(ES)
Guided Systems Technologies, Inc.
P. O. Box 1453
McDonough, GA 30253-1453

8. PERFORMING ORGANIZATION REPORT NUMBER

9. SPONSORING/MONITORING AGENCY NAME(S) AND ADDRESS(ES)
Department of the Air Force
Air Force Office of Scientific Research
4015 Wilson Blvd.
Arlington, VA 22203-1954

10. SPONSOR/MONITOR'S ACRONYM(S)

11. SPONSOR/MONITOR'S REPORT NUMBER(S)

12. DISTRIBUTION/AVAILABILITY STATEMENT

Distribution Statement: Approved for public release; distribution unlimited

20040324 049

13. SUPPLEMENTARY NOTES
DODAAD CODE:
Program Manager: Lt. Col. Sharon Heise

14. ABSTRACT

Successful operation of next-generation unmanned air vehicles will demand a high level of autonomy. Autonomous low-level operation in a high-threat environment dictates a need for on-hoard, robust, reliable and efficient trajectory optimization. in this report, we develop and demonstrate an innovative combination of traditional analytical and numerical solution procedures to produce efficient, robust and reliable means for nonlinear Light path optimization in the presence of time-varying obstacles and threats. The solution procedure exploits the natural time-scale separation that exists in the aircraft dynamics using singular perturbation theory. A reduced order problem involving only the kinematics of the position subspace is treated numerically. The nonlinear aircraft dynamics are to be treated analytically in phase II using a boundary layer analysis that results in an optimal feedback guidance solution. The developed algorithms were coupled with a neural network adaptive autopilot and integrated in an existing unmanned test-bed. This report documents the phase I effort, which produced a demonstration of the developed algorithm in near-real-time flight simulation, and included a simple evaluation of tracking computed trajectories on a rotary wing UAV.

15. SUBJECT TERMS

16. SECURITY CLASSIFICATION OF:			17. LIMITATION OF ABSTRACT	18. NUMBER OF PAGES	19a. NAME OF RESPONSIBLE PERSON
a. REPORT	b. ABSTRACT	c. THIS PAGE			Dr. J. Eric Corban
					19b. TELEPHONE NUMBER (Include area code) 770-898-9100

Report Documentation Page

On-Line Trajectory Optimization for Autonomous Air Vehicles

Technical Abstract

Successful operation of next-generation unmanned air vehicles will demand a high level of autonomy. Autonomous low-level operation in a high-threat environment dictates a need for on-board, robust, reliable and efficient trajectory optimization. In this report, we develop and demonstrate an innovative combination of traditional analytical and numerical solution procedures to produce efficient, robust and reliable means for nonlinear flight path optimization in the presence of time-varying obstacles and threats. The solution procedure exploits the natural time-scale separation that exists in the aircraft dynamics using singular perturbation theory. A reduced order problem involving only the kinematics of the position subspace is treated numerically. The nonlinear aircraft dynamics are to be treated analytically in phase II using a boundary layer analysis that results in an optimal feedback guidance solution. The developed algorithms were coupled with a neural network adaptive autopilot and integrated in an existing unmanned testbed. This report documents the phase I effort, which produced a demonstration of the developed algorithm in near-real-time flight simulation, and included a simple evaluation of tracking computed trajectories on a rotary wing UAV. The envisioned Phase II program will expand the scope of mission scenarios that can be addressed, will produce flight code validated in real-time hardware-in-the-loop simulation, and culminate in close range flight demonstration of the developed technology on a fixed-wing unmanned aircraft testbed.

List a Maximum of 8 Key Words that Describe the Project

Obstacle Avoidance
Singular Perturbation Theory
Guidance and Control
Trajectory Optimization
Optimal Guidance
Autonomous
Unmanned Air Vehicles
On-Line Path Planning

On-Line Trajectory Optimization for Autonomous Air Vehicles

Final Report
October 31, 2003

Report Number GST-03-4.5

Reporting Period: 9/1/02 – 9/1/03

STTR Phase I
Contract F49620-02-C-0085

Prepared for:

Dr. Belinda B. King
AFOSR/NM
4015 Wilson Blvd., Room 713
Arlington, VA 22203

phone: (703) 696-8409
email: belinda.king@afosr.af.mil

Prepared by:

J. Eric Corban, Eric N. Johnson, Anthony J. Calise, Shannon Twigg

Guided Systems Technologies, Inc.

P.O. Box 1453
McDonough, Georgia 30253-1453
Corban@mindspring.com
(770) 898-9100

ACKNOWLEDGEMENTS

The work presented herein was funded by the US Air Force Office of Scientific Research under STTR Phase I Contract F49620-02-C-0085. The phase I proposal was submitted in response to the 2002 Air Force STTR solicitation topic A02T002 entitled "Fast, Robust Real-Time Trajectory Generation for Autonomous and Semi-Autonomous Nonlinear Flight Systems." Many thanks to Ms. Shannon Twigg who supported the phase I effort while a graduate student at the Georgia Institute of Technology. The work reported herein also depends in part on previous research performed by P.K.A. Menon and his associates. Dr. Menon's discussion of this research topic with team members is much appreciated. Thanks also to Prof. Eric Johnson for his contribution of resources in the Georgia Tech School of Aerospace Engineering UAV lab that produced a demonstration of tracking a few simple obstacle avoidance trajectories using an unmanned helicopter during phase I.

TABLE OF CONTENTS

1. INTRODUCTION

1.1 PROBLEM/OPPORTUNITY

High-flying unmanned reconnaissance and surveillance systems are now being used extensively in the United States military. Current development programs will soon produce demonstrations of next-generation unmanned flight systems that are designed to perform combat missions. In practice, these vehicles must achieve a high level of autonomy in operations to be successfully deployed in large numbers. Their use in first-strike combat operations will dictate operations in densely cluttered environments that include unknown obstacles and threats, and will require the use of terrain for masking. The demand for autonomy of operations in such environments dictates the need for an on-board trajectory optimization capability.

1.2 OVERALL PROGRAM OBJECTIVE

The original phase I program solicitation establishes the overall program objective as:

"Develop, implement, and demonstrate algorithms for real-time trajectory generation of autonomous nonlinear flight systems. The algorithms must be capable of dealing with complex nonlinear vehicle dynamics, actuator and system constraints, as well as fixed and pop-up threats".

1.3 BACKGROUND ON TRADITIONAL METHODS

In any given mission scenario, the initial conditions, requirements, objectives, vehicle dynamics, and constraints can be analyzed at varying levels of detail to produce a number of feasible flight plans. However, in most situations conflicts will arise between the cited factors

that necessitate trade-off of one for the other. Ad hoc methods of solution can be constructed for simple missions with relatively few constraints, but such methods are quickly overwhelmed as problem complexity grows. In such cases formal methods for trajectory optimization are needed to identify a dynamically feasible solution that is "best" in some sense.

Methods available for solution of trajectory optimization problems generally fall into two distinct categories: direct and indirect. The former, which are numerical, seek to minimize or maximize the performance index directly by judicious choice of free parameters. The latter, for which analytic solutions can sometimes be derived, at least for problems of low order, seek to minimize or maximize the performance index indirectly by satisfying the first order necessary conditions for optimality that result from the application of the Calculus of Variations.

The direct approach first requires parameterization of the controls using discretization, spline fit, or the like. A parameter optimization algorithm is then employed to sequentially improve an initial guess of the state and control histories. Many such algorithms are in general use today and include variations on gradient and variable metric techniques.

The application of the necessary conditions for optimality (the indirect approach) generally results in a two-point boundary value problem (TPBVP). Analytic solutions are generally unobtainable except for problems of low order, and thus one must usually resort to numerical methods of solution. Nonlinear TPBVP are generally attacked using initial value or finite-difference methods. Initial value methods, often referred to as shooting methods,

continually satisfy the given initial conditions and the differential equations. A nominal solution is generated by guessing the missing initial conditions and integrating the differential equations forward in time. Bisection or other root-finding algorithms are then employed to reduce the cumulative error in the final conditions with each iteration. In contrast, finite-difference methods, also referred to as quasi-linearization methods, generally satisfy the initial and final conditions at each stage of the process while violating the differential equations to some degree. In between the pure shooting and finite difference methods fall the multi-point methods.

While great success has been achieved in numerically solving complex nonlinear trajectory optimization problems using direct and indirect techniques, many short comings still exist. Parameter optimization schemes tend to be tolerant of a poor initial guess but are in general slow to converge. Indirect methods, in contrast, can usually achieve greater accuracy in fewer iterations but also exhibit much greater sensitivity to the initial guess. Essentially all of the available methods in both categories demand computational resources that until recently were simply unavailable in a flight environment. For complex problem formulations with full vehicle dynamics, most have run times that preclude real-time mission updates. Almost all suffer from great complexity of implementation.

For these reasons, past aircraft trajectory generation studies were rooted in classical optimization theory and the calculus of variations. The focus was on up and away flight, with minimal concern for nap of the Earth maneuvering flight. A great variety of practical methods for optimizing the flight of aircraft both in two and three dimensions were developed in the

1960s and 70s. Much of this work began with the studies performed by Bryson based on minimizing time, fuel or range using reduced order modeling methods [1-3]. Subsequently, the use of singular perturbation methods, and multi-time scale analysis for trajectory optimization were suggested by Kelley [4,5], and later extensively developed and applied by Calise [6-9], Ardema [10] and others. A recent survey article may be found in [11]. In the work of Calise, the emphasis was on obtaining analytic or near-analytic feedback solutions that could be implemented with very limited computing resources in real-time.

Singularly perturbed dynamic systems are characterized by a small parameter multiplying the derivatives of some state vector components. If the parameter epsilon is set to zero, the order of the dynamic system is reduced. The solution to the reduced order problem that results when epsilon is set to zero provides the leading term in a perturbation series. Of course, the reduced order solution is not able to satisfy all the boundary conditions of the original full order problem. This is compensated for by constructing boundary layer transients that allow rapid variation of the fast states on a stretched time scale. The boundary layer solutions are required to satisfy the boundary conditions violated by the reduced solution and to approach the reduced solution asymptotically.

Natural time scale separation that exists in aircraft dynamics allows the successful application of singular perturbation methods to problems in atmospheric flight path optimization [12]. The reduced and boundary layer problems are often solvable using analytic methods alone.

This has made a unified analysis of 3-D high-performance aircraft path optimization possible [13].

1.4 PROPOSED INNOVATION

If we now consider flight of high performance aircraft at low levels where terrain and obstacles must be accounted for, the reduced order problem can no longer be solved in a purely analytic fashion. In this work, we exploit the natural time-scale separation in the flight vehicle dynamics, and the method of matched asymptotic expansions described above to analytically treat the nonlinear aircraft dynamics and associated constraints, and to address the path planning portion of the problem using numerical methods applied to only the kinematics in the x, y subspace. That is, numerical methods are used to solve the reduced order problem, and analytic solutions will be used to construct the boundary layer solutions. This novel approach builds on decades of previous work in efficient flight path optimization and real-time optimal guidance, and focuses the use of numerical solution procedures on only that portion of the problem for which fully analytic solutions are not available. The result is robust, autonomous, real-time optimal trajectory generation for nonlinear flight systems in complex mission scenarios.

2. REDUCED ORDER PROBLEM

In the early 1990s, P. K. Menon and Eulgon Kim researched methods of optimal trajectory path planning for terrain following and terrain masking flight. This research produced a reduced order formulation based on a constant velocity approach [14,15]. This chapter begins by expanding on the work done by Menon and Kim while using a constant energy approach.

2.1 A SIMPLIFIED FORMULATION

Consider the equations of motion for a flight vehicle written in a local level frame,

$$\dot{x} = V\cos\psi \tag{1}$$

$$\dot{y} = V\sin\psi \tag{2}$$

where x and y are the position coordinates, ψ is the heading angle (and also the control variable) and V is the horizontal component of velocity. If the vertical component of velocity is small, then V can approximately related to energy per unity mass (E) by

$$V = \sqrt{2g(E - f_1(x,y) - h_c)} \tag{3}$$

In this expression h_c is the ground clearance and $f_1(x,y)$ denotes the terrain altitude profile. Note that (3) embodies the constraint that the vehicle maintains a fixed height above the terrain. However, this is only approximately the case since V in this formulation is not the total velocity.

The cost equation is

$$J = \int_0^{t_f} [(1-K) + Kf(x,y)]dt \tag{4}$$

The function $f(x,y)$ denotes a combined penalty function of the terrain and threats. The weighting parameter, K, can vary between 0 and 1 and determines the amount of terrain masking and threat avoidance used in the optimization. When $K = 0$, the equations are optimized with respect to time. When K is set to 1, the path is optimized with respect to the threats and the terrain. For example, if $f(x,y) = f_1(x,y)$, then the path that minimizes the integrated altitude profile is found. More generally a weighted function of the terrain and threats will be employed, $f(x,y) = f_1(x,y) + f_2(x,y)$, where $f_2(x,y)$ is used to introduce a penalty for flying in the vicinity of a threat. Values of K between 0 and 1 correspond to a compromise solution.

The Hamiltonian equation is represented as

$$H = 1 - K + Kf(x,y) + \lambda_x V\cos\psi + \lambda_y V\sin\psi \tag{5}$$

Here, λ_x and λ_y are the costates. The differential equations for the costates are:

$$\dot{\lambda}_x = -\frac{\partial H}{\partial x} \tag{6}$$

$$\dot{\lambda}_y = -\frac{\partial H}{\partial y} \tag{7}$$

Evaluating these derivatives results in the expressions

$$\dot{\lambda}_x = -Kf_x + \frac{gf_{1x}}{V}\left[\lambda_x\cos\psi + \lambda_y\sin\psi\right] \tag{8}$$

$$\dot{\lambda}_y = -Kf_y + \frac{gf_{1y}}{V}\left[\lambda_x\cos\psi + \lambda_y\sin\psi\right] \tag{9}$$

In this expression, f_x, f_{1x} and f_y, f_{1y} denote the partial derivatives of $f(x,y), f_1(x,y)$ with respect to x and y, respectively. The optimality condition is

$$\frac{\partial H}{\partial \psi} = 0 \tag{10}$$

which results in

$$\tan\psi = \frac{\lambda_y}{\lambda_x} \tag{11}$$

In this formulation, the final time is free, and since the formulation is time invariant, $H = 0$ all along the trajectory. Using this fact together with (11), it is possible to obtain the following solutions for the costate variables

$$\lambda_x = \frac{-(1-K+Kf)\cos\psi}{V} \tag{12}$$

$$\lambda_y = \frac{-(1-K+Kf)\sin\psi}{V} \tag{13}$$

Taking the time derivative of (12) results in

$$\dot{\lambda}_x = \frac{-\left(Kf_x \dot{x} + Kf_y \dot{y}\right)V^2 \cos\psi}{V^3} - \frac{\left(f_{1x} \dot{x} + f_{1y} \dot{y}\right)(1-K+Kf)\cos\psi}{V^3} + \frac{(1-K+Kf)V\dot{\psi}\sin\psi}{V^3} \tag{14}$$

This expression can be used in (8) to solve for the heading angle rate

$$\dot{\psi} = \frac{A_5 \sin\psi + A_6 \cos\psi}{A_4 V} \tag{15}$$

where

$$A_5 = Kf_x V^2 + f_{1x} A_4 g \tag{16}$$

$$A_6 = Kf_y V^2 + f_{1y} A_4 g \tag{17}$$

$$A_4 = 1 - K + Kf \tag{18}$$

At this point, the problem to be solved has been reduced to three state equations (1), (2) and (15) to be solved, with only one unknown parameter to be determined, $\psi(0)$, the initial heading angle. Thus the family of extremals is parameterized by $\psi(0)$.

2.2 THE LOCAL TANGENT PLANE FORMULATION

Consider next a formulation that incorporates the constraint that the vehicle flies tangentially to the local terrain directly into the equations of motion. This is done by using the formulation in References 14 and 15 that starts out by writing the equations of motion in a local tangent frame. In the local tangent frame, the form of these equations become identical in form to (1) and (2), however V represents the total velocity in this formulation. Consequently the approximation embodied in the first formulation presented above is eliminated. After transformation to the local level frame, the equations motion become:

$$\dot{x} = \frac{V\cos\psi}{A_1} + \frac{Vf_x f_y \sin\psi}{A_1 A_2} \tag{19}$$

$$\dot{y} = \frac{-VA_1 \sin\psi}{A_2} \tag{20}$$

where,

$$V = \sqrt{2g(E - f(x,y) - h_c)} \tag{21}$$

$$A_1 = \sqrt{1 + f_x^2} \tag{22}$$

$$A_2 = \sqrt{1 + f_x^2 + f_y^2} \tag{23}$$

The control variable is still ψ, the local heading angle, and the cost equation is the same as stated in (4).

The Hamiltonian for this system becomes

$$H = 1 - K + Kf + \lambda_x \left[\frac{V \cos\psi}{A_1} + \frac{V f_x f_y \sin\psi}{A_1 A_2} \right] + \lambda_y \left[\frac{-V A_1 \sin\psi}{A_2} \right] = 0 \qquad (24)$$

and the costate equations are found to be:

$$\dot{\lambda}_x = -Kf_x + C_1 \left[C_2 + C_4 \sin^2\psi - C_3 \cos^2\psi + C_5 (\cos\psi)(\sin\psi) \right] \qquad (25)$$

$$\dot{\lambda}_y = -Kf_y + C_1 \left[C_6 + C_8 \sin^2\psi - C_7 \cos^2\psi + C_9 (\cos\psi)(\sin\psi) \right] \qquad (26)$$

where,

$$B_1 = f_{xx} f_y + f_x f_{xy} \qquad (27)$$

$$B_2 = f_{xx} f_x + f_y f_{xy} \qquad (28)$$

$$B_3 = f_{yy} f_y + f_x f_{xy} \qquad (29)$$

$$B_4 = f_{yy} f_x + f_y f_{xy} \qquad (30)$$

$$C_1 = \frac{A_4}{A_1^2 A_2^2 V^2} \qquad (31)$$

$$C_2 = -g f_x A_1^2 A_2^2 \qquad (32)$$

$$C_3 = A_2^2 V^2 f_x f_{xx} \tag{33}$$

$$C_4 = C_3 - A_1^2 V^2 B_2 \tag{34}$$

$$C_5 = A_2 V^2 \left(A_1^2 B_1 - 2 f_x^2 f_y f_{xx} \right) \tag{35}$$

$$C_6 = -g f_y A_1^2 A_2^2 \tag{36}$$

$$C_7 = A_2^2 V^2 f_x f_{xy} \tag{37}$$

$$C_8 = C_7 - A_1^2 V^2 B_3 \tag{38}$$

$$C_9 = A_2 V^2 \left(A_1^2 B_4 - 2 f_x^2 f_y f_{xy} \right) \tag{39}$$

The corresponding optimality condition is

$$\tan\psi = \frac{\lambda_x f_x f_y - \lambda_y A_1^2}{\lambda_x A_2} \tag{40}$$

Following the same procedure as described for the simplified formulation above, (24) and (40) can be used to solve for λ_x and λ_y:

$$\lambda_x = \frac{-A_4 A_1 \cos\psi}{V} \tag{41}$$

$$\lambda_y = \frac{A_4 \left(A_2 \sin\psi - f_x f_y \cos\psi \right)}{V A_1} \tag{42}$$

Taking the time derivative of (41) and setting it equal to (25) yields the following expression for the heading angle rate:

$$\dot{\psi} = \frac{D_1 \sin\psi + D_2 \cos\psi}{D_3} \tag{43}$$

where:

$$D_1 = A_2 V^3 f_x E_3 - A_1^2 A_4 E_4 \tag{44}$$

$$D_2 = f_x^2 f_y E_1 - A_1^2 V f_y E_2 \tag{45}$$

$$D_3 = A_1^3 A_2 A_4 V^2 \tag{46}$$

$$E_1 = A_1^2 V^3 K - A_4 V^3 f_{xx} + g A_1^2 A_4 V \tag{47}$$

$$E_2 = A_1^2 K + g A_1^2 A_4 - A_4 V^2 f_{xx} \tag{48}$$

$$E_3 = A_4 f_{xx} - A_1^2 K \tag{49}$$

$$E_4 = g A_2 V f_x + \frac{B_2}{A_2} \tag{50}$$

As with the previous formulation, the system is now reduced to solving three differential equations with one unknown parameter, the initial heading.

2.3 INTRODUCING A HEADING RATE CONSTRAINT

A constraint on the heading rate can be incorporated by introducing the equation

$$\dot{\psi} = u \tag{51}$$

where u is the new control variable. The heading rate constraint is modeled by imposing the following constraint on u

$$|u| \leq c \tag{52}$$

The constraint is adjointed to the Hamiltonian by using constraint multipliers. This results in

$$H = 1 - K + Kf + \lambda_x \dot{x} + \lambda_y \dot{y} + \lambda_\psi u + \mu_1(u - c) + \mu_2(-u - c) \tag{53}$$

In this expression, λ_ψ is the costate variable corresponding to the newly introduced ψ state, and μ_1 and μ_2 and are multipliers used to impose the upper and lower limits on the heading rate. When the control is not on one of the constraints, μ_1 and μ_2 are both equal to zero. When the control is on one of the constraints, the corresponding multiplier is positive.

When not on the constraint we have a *singular* solution

$$\frac{\partial H}{\partial u} = 0 = \lambda_\psi \tag{54}$$

which further implies that $\dot{\lambda}_\psi = 0$. The differential equations for the costates are found from the following relations:

$$\dot{\lambda}_x = -\frac{\partial H}{\partial x} \tag{55}$$

$$\dot{\lambda}_y = -\frac{\partial H}{\partial y} \tag{56}$$

$$\dot{\lambda}_\psi = -\frac{\partial H}{\partial \psi} = 0 \tag{57}$$

Equations (55) and (56) are the same as those obtained earlier in (8) and (9) or (25) and (26), and (57) reduces to the optimality conditions in (11) or (40). Therefore, the portion of the trajectory in which the constraint is not on the limit may be solved the same way as described earlier for the unconstrained case.

When the optimality conditions result in a solution that violates the upper limit, $\mu_2 = 0$, while $\mu_1 \geq 0$ and the new optimality equation is

$$\frac{\partial H}{\partial u} = 0 = \lambda_\psi + \mu_1 \tag{58}$$

which results in the relationship

$$\lambda_\psi = -\mu_1 \tag{59}$$

The Hamiltonian can then be written as

$$H = 1 - K + Kf + \lambda_x \dot{x} + \lambda_y \dot{y} + \lambda_\psi c \tag{60}$$

The differential equations for λ_x and λ_y remain unchanged while the differential equation for λ_ψ is found to be

$$\dot{\lambda}_\psi = \lambda_x V \sin\psi - \lambda_y V \cos\psi \tag{61}$$

or

$$\dot{\lambda}_\psi = \frac{\lambda_x V\left(A_2 \sin\psi - f_x f_y \cos\psi\right) + \lambda_y V A_1 \cos\psi}{A_1 A_2} \tag{62}$$

for the first and second formulations, respectively. This results in a system of six differential equations that must be solved for along a constrained arc. When the problem solution does not begin on a constraint, there are no unknown parameters to be found when a constraint is hit. All of the initial conditions are equal to their respective values at the point of entering the constraint, which can be easily calculated. However, if the solution begins on the constraint, the initial conditions for the three costate differential equations -- equations (55), (56) and (57) -- must be solved for.

The constrained solution for the case where the unconstrained solution violates the lower limit mirrors the constrained solution obtained for the case where it violates the upper limit. The only difference is in the optimality condition.

$$\frac{\partial H}{\partial u} = 0 = \lambda_\psi - \mu_2 \tag{63}$$

which yields the relationship

$$\lambda_\psi = \mu_2 \tag{64}$$

Here the new Hamiltonian can be written as

$$H = 1 - K + Kf + \lambda_x \dot{x} + \lambda_y \dot{y} - \lambda_\psi c \tag{65}$$

2.4 FORMULATING THE ALPHA LIMIT

Another possible method of constraining the turn rate is through the analysis of the alpha -- or angle-of-attack -- limit. The equations for heading and flight path angle rate are:

$$
\begin{aligned}
mV\dot{\psi} &= L\sin\mu / \cos\gamma \\
mV\dot{\gamma} &= L\cos\mu - W\cos\gamma
\end{aligned}
\tag{66}
$$

where V is the total velocity, ψ is the heading, γ is the flight path angle, L is the lift, μ is the bank angle, and m is the mass. In low speed flight, the turn rates in (66) are limited by the stall angle of attack. The lift limit that results from a limit on angle of attack is given by

$$
\overline{L} = qS\overline{C}_L = qSC_{L\alpha}\overline{\alpha} \tag{67}
$$

where the overbar indicates a limit value. Note that since q is a quadratic function of V, (66) implies that for given alpha, both heading rate and flight path increase linearly with velocity. Thus, if the flight speed is already being maintained as high as possible, maintaining a commanded heading rate when on the alpha limit by using throttle control is not an option.

Assuming that throttle is used to maintain constant energy, the expression for the first and second time derivatives of altitude are:

$$
\begin{aligned}
\dot{h} &= V\sin\gamma \\
\ddot{h} &= -g\sin^2\gamma + V\cos\gamma\dot{\gamma}
\end{aligned}
\tag{68}
$$

The second equation in (68) can be used to solve for the flight path angle rate needed to follow the terrain, where γ and $\ddot{h}$ are related to the terrain data using

$$\sin\gamma = (f_x\dot{x} + f_y\dot{y})/V$$
$$\ddot{h} = f_x\ddot{x} + f_y\ddot{y} + f_{xx}\dot{x}^2 + (f_{xy} + f_{yx})\dot{x}\dot{y} + f_{yy}\dot{y}^2 \tag{69}$$

Note that the second equation in (69) together with the second equation in (68) establish an algebraic constraint on $\dot{\gamma}$ so long as f_x and f_y do not simultaneously vanish. Consequently, viewing alpha as the fundamental limit results in a limit on $\dot{\psi}$ through (66) that is a complex function of x, y and ψ. Therefore, the corresponding costate equations become significantly more complex when the alpha constraint becomes active. This is in contrast to the situation described so far in this paper, where the x and y costate equations remain the same when on the heading rate limit.

2.5 Introducing Velocity as a Control Variable

The constant energy formulation was originally introduced as a potentially more realistic formulation than the constant velocity formulation of Ref. 17, particularly for vehicles with low thrust to weight ratio. However, a deficiency of the constant energy formulation is that it results in low velocities at high altitude and high velocities at low altitude, the opposite of what might be expected for a realistic trajectory. In a practical system, the velocity profile would be controlled to provide the highest possible airspeed during periods of straight flight. The question becomes how velocity should be regulated during periods of maneuvering flight. As noted above, if the aircraft is angle of attack limited, then the maximum turn rate increases linearly

with velocity. However, for terrain following, it can be argued that turn radius is of greater concern than turn rate. Since turn radius (R) is related to turn rate ($\dot{\phi}$) and velocity (V) by

$$R\dot{\phi} = V \tag{70}$$

it follows that the minimum turn radius is independent of velocity. Thus is would appear that the constant velocity formulation of Ref. 14 would be appropriate for vehicles whose turn radius is angle of attack limited. However, vehicles capable of high-speed flight are typically load factor limited above a speed known as the corner velocity. The corner velocity is defined by the condition

$$\overline{L} = qSC_{L_\alpha}\overline{\alpha} = \frac{\rho V^2 SC_{L_\alpha}\overline{\alpha}}{2} = W\overline{G} \tag{71}$$

where $\overline{\alpha}$ is the alpha limit and $\overline{G}$ is the load factor limit. Solving (71) for the corner velocity we get

$$V_c = \sqrt{\frac{2W\overline{G}}{\rho SC_{L_\alpha}\overline{\alpha}}} \tag{72}$$

The corner velocity can vary significantly depending on the vehicle characteristics and its limits.

This section considers a new formulation in which both V and turn rate are treated as a

control variable. To simplify the formulation of the turn rate limit, the effect of gravity is ignored, and all turning is assumed to take place in the horizontal plane. A more detailed formulation is described above in the section *Formulating the Alpha Limit*, however it is not clear at this stage if that formulation will be tractable. To further simplify the presentation, the treatment is limited to the simplified formulation in which the vertical component of velocity is ignored in the dynamics. The dynamics are:

$$\begin{aligned} \dot{x} &= V\cos\psi \\ \dot{y} &= V\sin\psi \\ \dot{\psi} &= u \end{aligned} \tag{73}$$

The constraints are:

$$\begin{aligned} \underline{V} \le V \le \overline{V} \\ |u| \le \bar{u}(V) \end{aligned} \tag{74}$$

It is assumed that the upper and lower limits on V are constant. The upper limit on u is velocity dependent, and follows from the approximation (ignoring gravity)

$$\bar{u} = \overline{L} / mV \tag{75}$$

Thus it follows from (71) and (72) that

$$\bar{u}(V) = \begin{cases} \dfrac{\rho C_{L_\alpha} \bar{\alpha}}{2m}, & V \le V_c \\ \dfrac{g\bar{G}}{V}, & V > V_c \end{cases} \tag{76}$$

Note that $\bar{u}(V)$ is independent of V when $V < V_c$ and that $d\bar{u}/dV$ is discontinuous at $V = V_c$. Clearly, from the earlier discussion, this formulation is only needed for the case $\bar{V} > V_c$, otherwise from the perspective of minimizing the time of flight, there is no advantage to flying at any speed less that $\bar{V}$. We further assume that $\underline{V} < V_c$. Then it is fairly safe to assume that the lower limit on V is never active, since there is no advantage to flying at a velocity less than $\bar{V}$. With this reasoning, it also follows that only the lower expression for $\bar{u}(V)$ applies.

The performance index is the same as that described earlier

$$J = \int_0^{t_f} [(1-K) + Kf(x,y)]dt \tag{77}$$

where the final time is free. Thus the Hamiltonian for this system satisfies

$$H = 1 - K + Kf(x,y) + \lambda_x V \cos\psi + \lambda_y V \sin\psi + \lambda_\psi u + constraints = 0 \tag{78}$$

The constraint terms can be expressed as

$$constraints = \mu_1(u^2 - \bar{u}^2) + \mu_2(V - \bar{V}) \tag{79}$$

Both constraint terms are written in a form such that the quantities in parenthesis are negative when the constraints are not active. Therefore $\mu_i \geq 0$ when the ith constraint is active, and $\mu_i = 0$ when ith constraint is inactive . It is apparent from (78) that when the constraint on u is inactive, H is a linear function of both V and u. Therefore the optimal solution for V is either at its limit, or is singular. Since final time is a component in the performance index, it is probably safe to rule out the possibility that a singular arc in V is optimal. Therefore, we assume that when the constraint on u is inactive, the optimal solution for V is $V^* = \overline{V}$. Furthermore, when the constraint on u is inactive it follows that the optimal solution for u is singular, in which case we have that along a singular arc:

$$\begin{aligned} \frac{d}{dt} H_u &= \lambda_\psi(t) = 0 \\ \frac{d^2}{dt^2} H_u &= \dot{\lambda}_\psi = -H\psi = 0 \end{aligned} \tag{80}$$

The conditions in (80) can easily be used to deduce the fact that the trajectory equations defining an extremal arc can be derived using the same approach as above, with the simplification that V is constant. The same conclusion can be reached for the tangent plane formulation. Therefore, when the constraint on u is inactive, the equations are simpler in form than those above, and reduce to the equations in Ref. 14 for the tangent plane formulation.

When the constraint on u is active, then $|u| = g\overline{G}/V$ and the optimal value for V follows from the optimality condition:

$$H_V \equiv \frac{\partial H}{\partial V} = \lambda_x \cos\psi + \lambda_y \sin\psi + \mu_1 \frac{2(g\overline{G})^2}{V^3} = 0 \qquad (81)$$

Now (81) applies only when the resulting solution (V^*) satisfies $V^* > V_c$, since as noted earlier, $\overline{u}(V)$ has a corner (discontinuous first derivative) at $V = V_c$. If (81) results in a solution that is less than V_c, then the minimum for H occurs at $V^* = V_c$. The multiplier μ_1 can be related to λ_ψ using

$$H_u = \lambda_\psi + \frac{2\mu_1 g\overline{G}}{V}\mathrm{sgn}(u) = 0 \qquad (82)$$

Note that since $\mu_1 \geq 0$, it follows from (82) that $\mathrm{sgn}(u) = -\mathrm{sgn}(\lambda_\psi)$. Combining (81) and (82) we have

$$V^* = \sqrt{\frac{-g\overline{G}|\lambda_\psi|}{\lambda_x \cos\psi + \lambda_y \sin\psi}}, \quad V^* > V_c \qquad (83)$$

otherwise $V^* = V_c$. Combining (78), (81) and (82) with the fact that $|u| = g\overline{G}/V$ when the constraint is active, results in

$$H = 1 - K + Kf(x,y) + 2(\lambda_x V \cos\psi + \lambda_y V \sin\psi) = 0 \tag{84}$$

Using the Hamiltonian equation shown in equation (84), the following costate differential equations can be determined

$$\begin{aligned} \dot{\lambda}_x &= -Kf_x \\ \dot{\lambda}_y &= -Kf_y \\ \dot{\lambda}_\psi &= -\frac{\partial H}{\partial \psi} \end{aligned} \tag{85}$$

This leads to the equation for $\dot{\lambda}_\psi$.

$$\dot{\lambda}_\psi = -2V(\lambda_y \cos(\psi) - \lambda_x \sin(\psi)) \tag{86}$$

These equations can then be integrated to find the solution. As in the heading rate constraint section, the initial conditions for the costates are known when the overall solution does not start on the constraint. Otherwise, the initial conditions must be solved for.

In a similar fashion, the corresponding equations for the local tangent plane formulation can be derived. For this section, the state equations are

$$\begin{aligned} \dot{x} &= M_1 V \\ \dot{y} &= -M_2 V \\ \dot{\psi} &= u \end{aligned} \tag{87}$$

where

$$M_1 = \frac{\cos(\psi)}{A_1} + \frac{f_x f_y \sin(\psi)}{A_1 A_2} \tag{88}$$

$$M_2 = \frac{A_1 \sin(\psi)}{A_2} \tag{89}$$

A_1 and A_2 are defined in equations (22) and (23). These equations lead to a Hamiltonian equation of

$$H = 1 - K + Kf(x,y) + \lambda_x VM_1 + \lambda_y VM_2 + \lambda_\psi u + constra\,\text{int}\,s = 0 \quad (90)$$

with the constraint term given in equation (79) above.

As described previously, when the constraint on the heading rate is not met, the problem simplifies to the constant velocity formulation described in Ref. 14 using the maximum velocity. For the case when the constraint is hit, the optimality conditions are

$$H_V \equiv \frac{\partial H}{\partial V} = \lambda_x M_1 - \lambda_y M_2 + \mu_1 \frac{2(g\bar{G})^2}{V^3} = 0 \quad (91)$$

$$H_u = \lambda_\psi + \frac{2\mu_1 g\bar{G}}{V}\text{sgn}(u) = 0 \quad (92)$$

These equations can then be combined to find the following optimal velocity

$$V^* = \sqrt{\frac{-g\bar{G}|\lambda_\psi|}{\lambda_x M_1 - \lambda_y M_2}}, \qquad V^* > V_c \quad (93)$$
$$V^* = V_c, \qquad V^* \le V_c$$

Combining (90), (91) and (92) result in the following new Hamiltonian equation.

$$H = 1 - K + Kf(x,y) + 2V(\lambda_x M_1 + \lambda_y M_2) = 0 \quad (94)$$

Equation (90) is used to evaluate the last expression in (85).

$$\dot{\lambda}_\psi = -2V(\lambda_x N_1 - \lambda_y N_2) \quad (95)$$

with

$$N_1 = \frac{-\sin(\psi)}{A_1} + \frac{f_x f_y \cos(\psi)}{A_1 A_2} \tag{96}$$

$$M_2 = \frac{A_1 \cos(\psi)}{A_2} \tag{97}$$

3.0 NUMERICAL RESULTS

3.1 MODEL USED FOR GENERIC TESTING

A sample trajectory was generated for both the simplified and local tangent plane formulations described above. In both cases, the path was from the initial point (-10, -10) to a final point (10, 10). The terrain was generated from the function

$$z = .5\cos(.4x)\sin(.3y) + 1 \tag{98}$$

and the function $f(x,y)$ was chosen to equal $f_1(x,y)$. The trajectories found with each formulation are essentially identical. Figure 1 below shows the path over the terrain for K=1 while Figure 2 shows the trajectory for K=0. In Figure 2, this path is basically a straight line. In Figure 1 it can be seen that the trajectory winds around the hills.

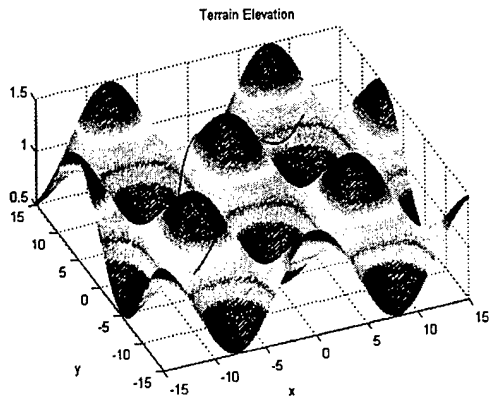

Figure 1: (-10, -10) to (10,10): K=1

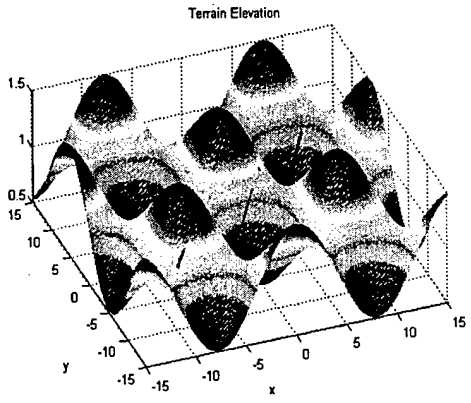

Figure 2: (-10, -10) to (10,10): K=0

Although the trajectories are nearly identical, this does not imply that the simplified formulation can be used in place of the tangent plane formulation with negligible effect on the guided solution when the full aircraft dynamics are taken into account. This can only be assessed using a higher fidelity simulation of the aircraft motion.

3.2 REAL TERRAIN DATA

To increase the realism of this model, real terrain data was acquired from the United States Geological Survey to incorporate into this model [16]. The data was found in tabular format relating the altitude to the locations longitude and latitude, with data points spaced approximately every 48 feet. This data was then converted to matrix form, from which it could then be used as $f_1(x,y)$. Because of the distance between the sampled altitude points in the matrix, the data was then smoothed to appear more continuous and to remove the discontinuous leaps in altitude. The gradients of this matrix, along both the x and y directions, were calculated numerically to form matrices representing $f_{1x}(x,y)$ and $f_{1y}(x,y)$. The gradients of these two matrices yielded matrices for $f_{1xx}(x,y)$, $f_{1yy}(x,y)$ and $f_{1xy}(x,y)$.

For this portion of the testing, it was decided to use a section of terrain near Columbus, Ohio. A profile of this terrain can be seen in Figure 4. In this graph, the x and y axes depict the position coordinates, measured in feet, such that the x axis point north and the y axis points west. The altitude of the terrain is measured along the z-axis and is also given in feet. This plot depicts a square plot of land, with 10,000 feet to a side. The measurements along the x and y

axes are relative to a set origin for the terrain data collected; this plot is just one small piece.

3.3 TERRAIN PATH RESULTS

Some initial results using actual terrain data have been investigated using the simplified formulation described above. The energy, which is stated and held constant through the calculations, was found by determining the energy needed to fly the vehicle at its minimum speed at the highest altitude position in an area near the flight path. This

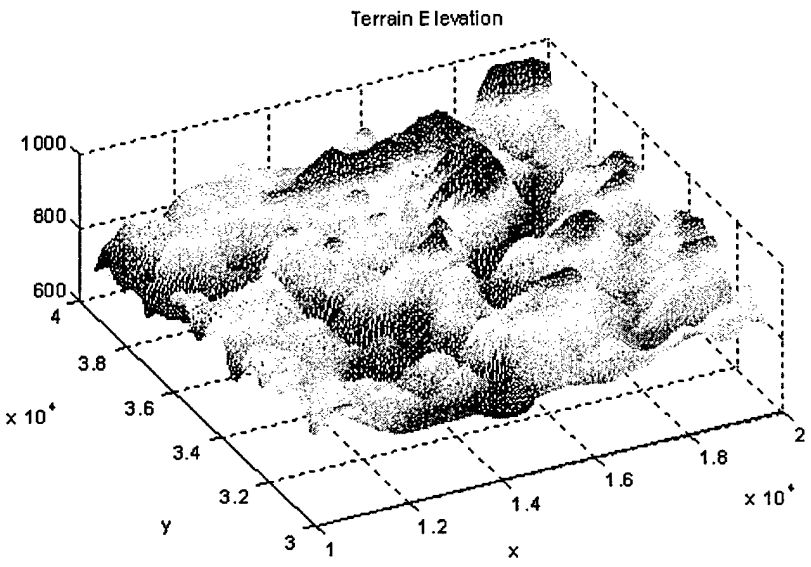

Figure 4: Terrain Plot of an Area Near Columbus Ohio

ensures that the necessary velocity for flight is never smaller than the minimum. However, if the change in altitude is too large, the velocity of the plane can exceed its upper bounds at lower altitudes, so a velocity constraint will need to be implemented.

Some flight paths have been computed using the simplified formulation outlined above. Initial results from this can be seen in Figures 5 and 6. In Figure 5, it can be seen that a flight trajectory is outlined from the point (15500,34000) to (18300,31800) -- this entails a flight of 3561 feet. Figure 6 shows a trajectory of 3688 feet from the point (18000, 34100) to (15200, 31700). In both plots, the black trajectory represents K = 1 while the purple trajectory is for the case K = 0.

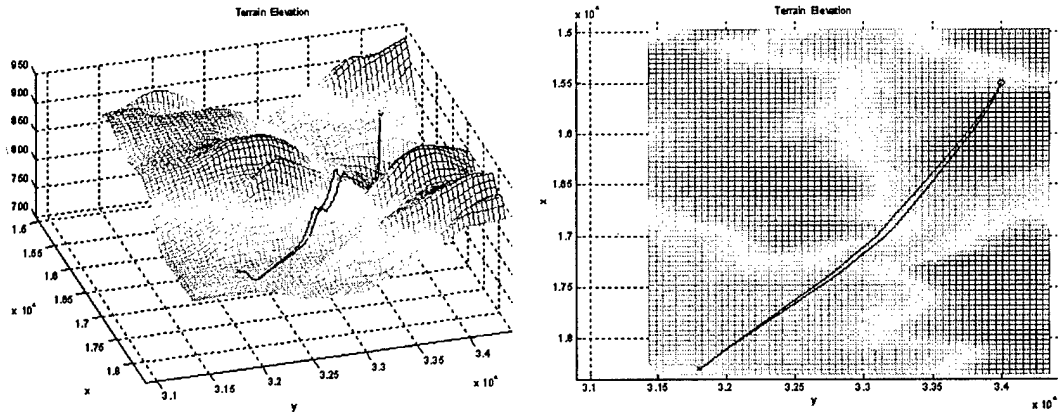

Figure 5: Sample Flight Path from (15500,34000) to (18300,31800) Using Simplified Formulation. Black line represents K=1 and Purple line represents K=0.

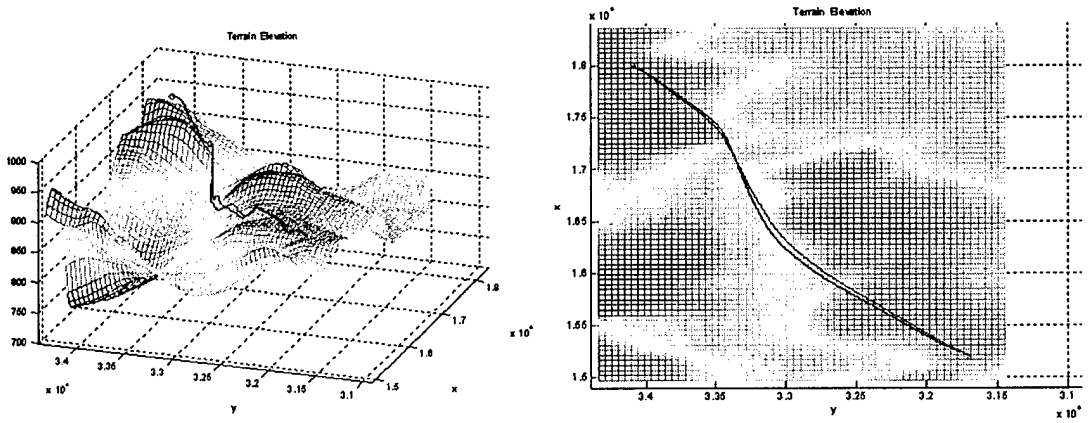

Figure 6: Sample Flight Path from (18000,34100) to (15200,31700) Using Simplified Formulation. Black line represents K=1 and Purple line represents K=0.

Figure 7 depicts trajectories created from the local tangent plane formulation. The two plots are for the same initial and final conditions as those shown in Figures 5 and 6. The results for the two formulations are very similar. Figure 8 shows a comparison of the results of the two formulations. In these plots, the red line indicates the results from the local tangent plane formulation while the black line represents the simplified form.

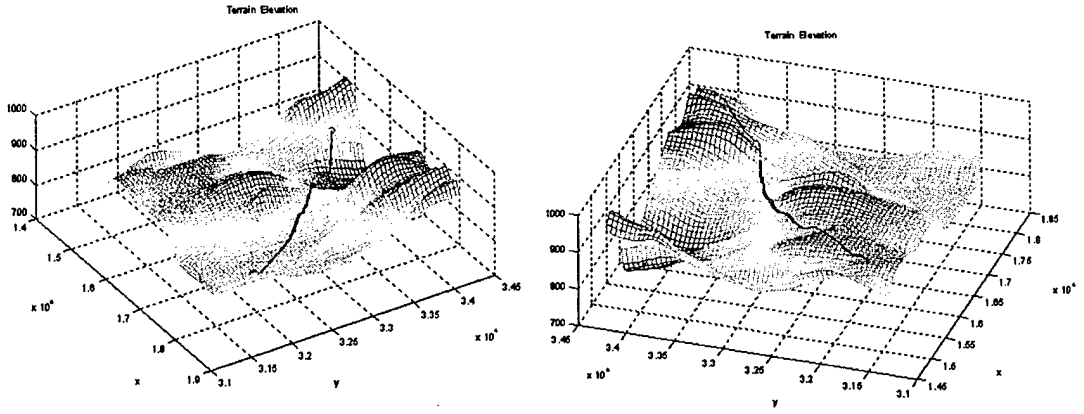

Figure 7: Sample Flight Paths from (15500,34000) to (18300,31800) and (18000,34100) to (15200,31700) Using Local Tangent Plane Formulation. Black line represents K=1 and Purple line represents K=0.

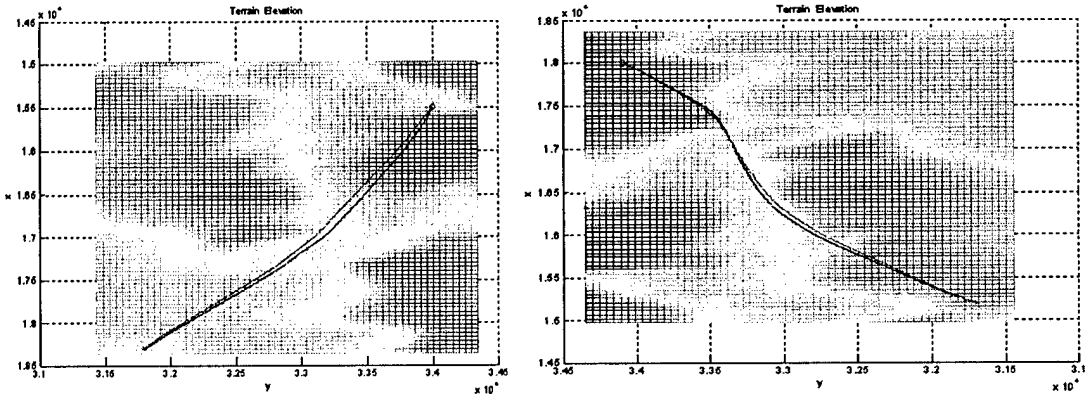

Figure 8: Sample Flight Paths from (15500,34000) to (18300,31800) and (18000,34100) to (15200,31700) Using K=1. Black line represents Simplified Formulation and Red line represents Local Tangent Plane Formulation.

In addition, as can be seen in the figures, the trajectories for both K = 0 and K = 1 are similar. This is because a minimum time approach with constant energy will also work to minimize the altitude of flight, to some extent, due to the fact that the velocity of the vehicle will be greater at lower altitudes.

3.4 Modified Constant Energy Approach

When using the constant energy formulation, the velocity changes greatly during a flight, as has been mentioned earlier. This can lead to solutions that are not flyable. To correct this default, a modified constant energy formulation is implemented which utilizes a slightly modified definition of the velocity. The velocity definition, which can be seen in equation (3), is a direct function of the position through the terrain altitude. The modified velocity is also a function of the position through the altitude via the equation

$$V = V_{nom} + f\left(h_{hp}(x,y)\right) \tag{99}$$

where V_{nom} is a given nominal velocity and $f(h_{hp}(x,y))$ is velocity component found through a high-pass filter of the overall terrain. With this formulation, the velocity will remain closer to a constant value, but will have some fluctuations due to short term changes in the altitude.

The trajectories found using this modification closely match the previous solutions, but with a more favorable velocity profile. Comparisons between the full constant energy approach and

the modified format can be seen below in Figure 9. This figure shows the results using the simplified equations of motion. The left hand plot depicts the trajectory found for this situation. The path is identical for the two formulations used. The plot on the right shows the velocity versus time for the two cases. The blue line is the velocity for the original constant energy formulation while the green line represents the velocity from the modified constant energy formulation. It can be seen that the green velocity varies much less while the necessary time for the trajectories is very similar.

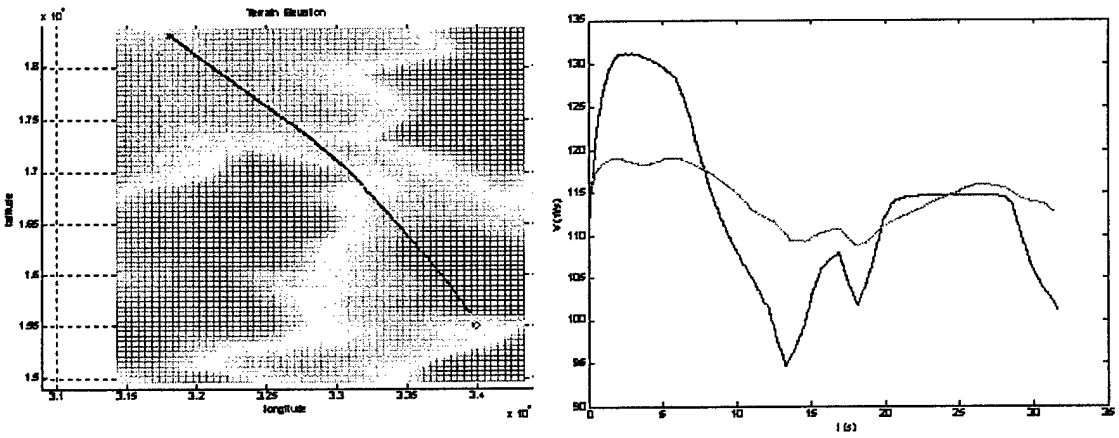

Figure 9: Sample Flight Path from (15500,34000) to (18300,31800) comparing results from Original and Modified Constant Energy Formulations. Left side shows path. Right side shows velocities versus time with blue line representing original form while green line represents modified form.

3.5 Implementation of a Heading Constraint

A heading constraint has also been successfully implemented for the constant velocity approach described in Ref. 14. Results for this can be seen below in Figure 10. This result is using the simplified formulation with the heading rate limited to 0.02 radians/second – the

unconstrained heading rate had a maximum of about 0.035 radians/second. The left side of the figure shows the plot of the trajectory found. The right side shows a plot of the heading rate versus time. In this plot, it can be seen that the heading rate constraint is reached at the beginning of the trajectory as well as two other times during the course of the flight.

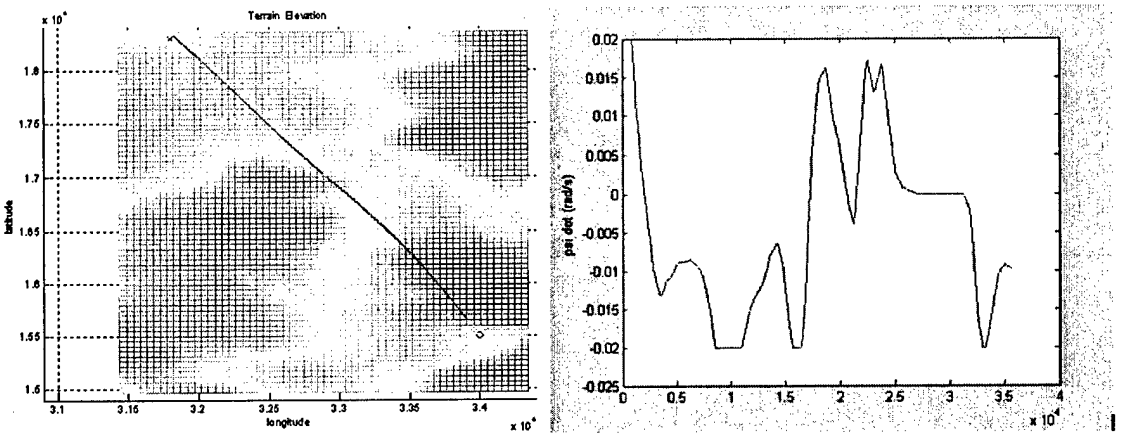

Figure 10: Sample Flight Path from (15500,34000) to (18300,31800) implementing a Constant Heading Rate Constraint on the Simplified Constant Velocity Formulation. Left side shows path. Right side shows heading rate versus time.

3.6 Flight Testing and Simulator Implementation

The optimal path planning code using the local tangent plane formulation was tested first on the Georgia Tech helicopter simulator and then in actual flight tests with the helicopter. The simulator was tested first to ensure the paths determined were flyable on an actual aircraft, before the flight tests. At the same time, the threat avoidance portion of the code was tested. As can be seen in above in equations (3) and (4), there are two different terms regarding terrain-type inputs. One is solely the terrain while the other is a combined penalty function of the terrain and threats. Previously, it was assumed that these two functions were the same – this meant there were no

threats other than the terrain. Ideally, the optimal path would avoid all the threats and weave between them.

The vehicle used for these tests was a Yamaha R-Max helicopter, seen in Figure 11 below. This helicopter weighs about 66 kilograms and has a three-meter rotor. It is capable of flying between approximately 30 – 80 feet per second. In addition, it can fly predetermined paths autonomously.

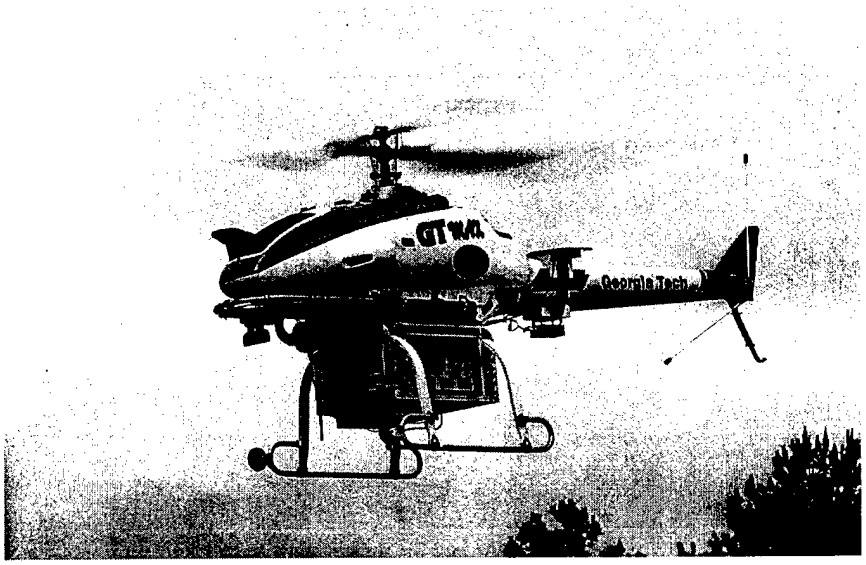

Figure 11: Georgia Institute of Technology
GT-Max Helicopter

To test the threat avoidance capabilities, new terrain data files were generated that used a mostly flat terrain with threats imposed on it as large hills. Two different methods of generating these hills were tested. The first was using sine functions in the following form

$$f = A\sin(b * x)\sin(c * y) \tag{100}$$

Here A is the amplitude of the hill, b and c are scaling factors to adjust the width of the hill and x

and y are the coordinates along the hill. Figure 12 shows one case with this representation. It was found that this form of creating the hills was not successful. As can be seen in equation (43), the heading rate is dependent on the gradients of the terrain function. Therefore, the only place where the heading angle would change to circle the threat is when the path touches the edge of the threat. However, no matter what the height or width of the hill was, the effect of touching the edge of the threat was to cause the path to veer over the top of the hill.

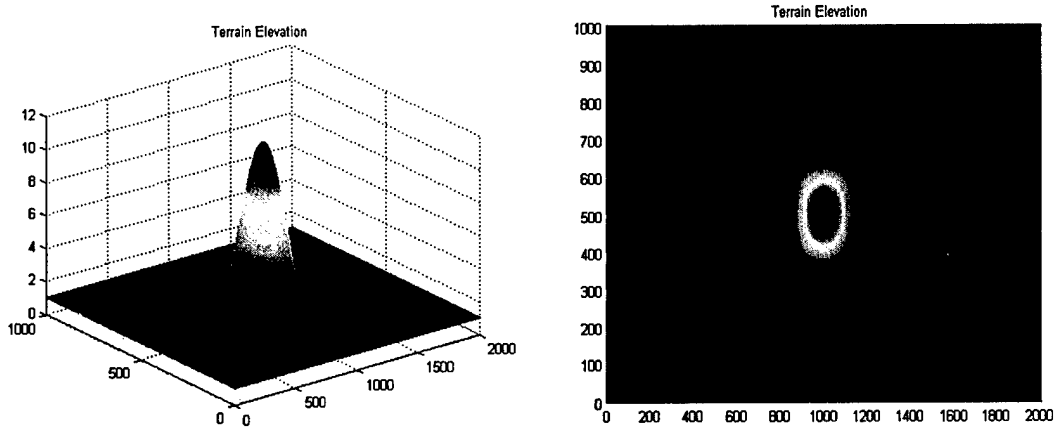

Figure 12: Terrain with threats formulated as a sine function.
On the right is an overhead view.

The next method of generating the terrain involved using an exponential function in the form

$$f = Ae^{-r^2/b} \tag{101}$$

where A is the amplitude, b is a scaling factor to adjust the width and r is the distance from any position to the center of the threat. A plot of this representation can be seen in

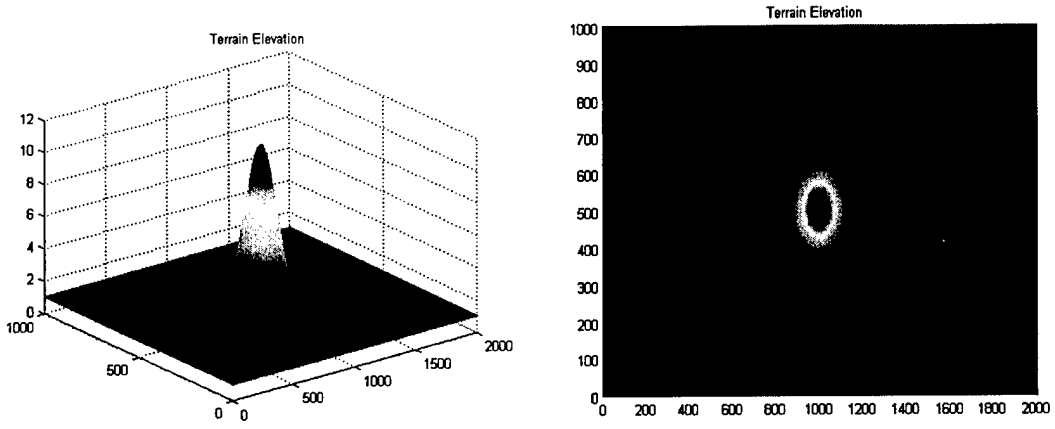

Figure 13: Terrain with threats formulated as an exponential function.
On the right is an overhead view.

Figure 13. This formulation actually affects the entire terrain plot slightly, so the terrain gradients are nonzero for a large portion of the time as with the sine function form. Consequently, the transition between the flat terrain and the hills are less abrupt. This allows the program to find a solution that avoids the threats.

Three different scenarios were tested in increasing levels of difficulty. The first included a single threat in the middle of the field, as depicted above in Figure 13. The second then used three threats while the third included five threats. In all cases, the threats were given a diameter of about 300 feet and amplitude of ten feet. This amplitude of ten feet was chosen because it is easily scalable to any desired amplitude. The dimensions of the field used were 1000 feet in the x-direction pointing north and 2000 feet in the y-direction pointing east. In the second case, the three threats were located at: (600,1000), (800,1600), and (200,500). In the third case, the locations of the threats were: (500,1000), (700,1400), (300,1600), (750,400), and (200,300). The terrain used for the second and third cases can be seen below in Figure 14.

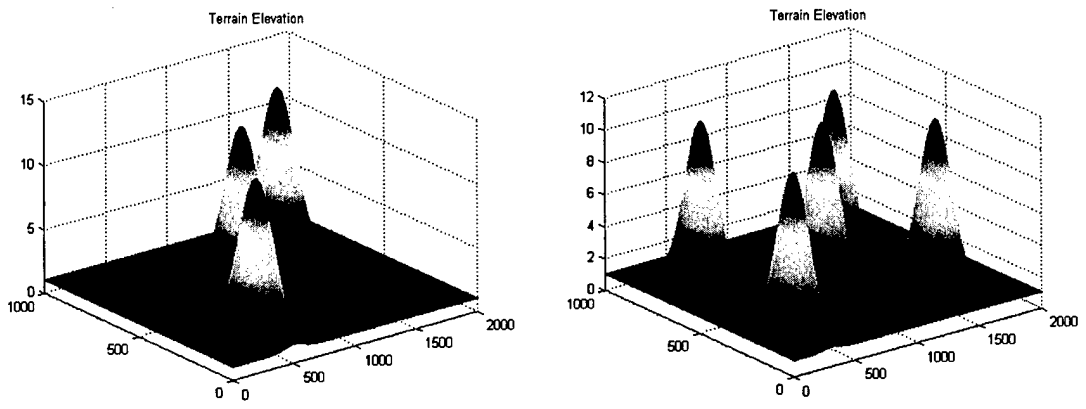

Figure 14: Terrain used in the simulations. The left side shows the terrain with three threats. The right side shows the terrain with five threats.

For the purposes of these simulator and flight tests, the local tangent plane formulation using a constant velocity was used. This was decided because the terrain was flat – other than the threats – which would result in the velocity from the constant energy formulation being constant. A velocity of 40 feet per second was chosen to use with this helicopter. The results for the three tests can be seen below. In each of the plots, the black line represents the trajectory found by the program while the blue line is the actual path flown by the helicopter during the flight tests. In each case, the starting position for the path was at the point (500,1800) while the final position for the path was at (500,200). In addition, the actual flight path, the blue line, extends beyond these points. This portion of the flight was used to accelerate and decelerate the vehicle so that the entire planned path between the starting and ending points was flown at a constant 40 feet per second.

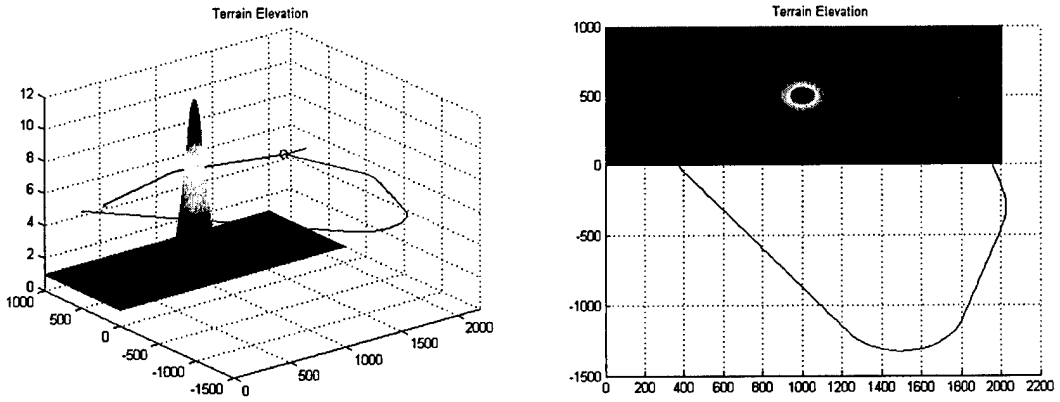

Figure 15: Flight paths from first case. The black line is the commanded path and the blue line is the actual path.

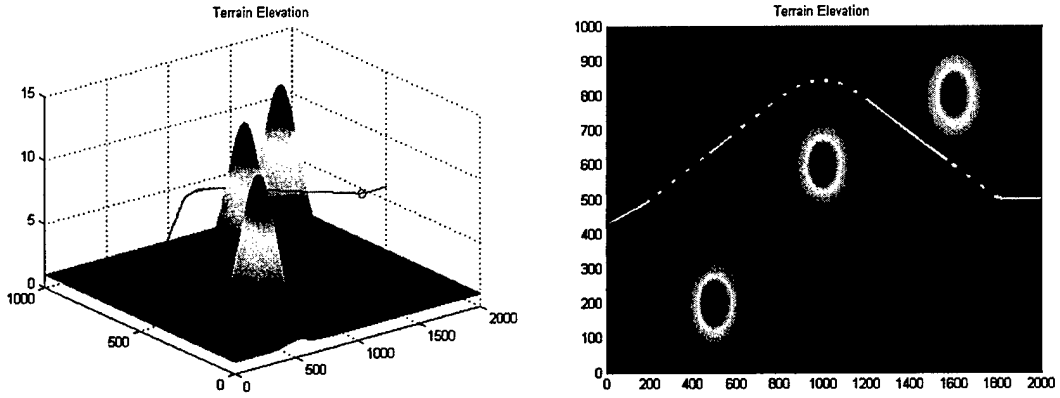

Figure 16: Flight paths from second case. The black line is the commanded path and the blue line is the actual path.

The flight results for the first case can be seen in Figure 15. This case did not appear to produce good results. However, the problem was with an axes error. The wrong file was uploaded to the helicopter – one with the axes rotated. So, in this case, the correct relative trajectory was flown, just in the wrong direction. Instead of proceeding west, the helicopter turned south and flew the predetermined path in that direction; then it continued to fly to its

planned ending point. The results to the second and third cases can be seen in Figures 16 and 17. In both of these cases, the actual flight results match the optimal trajectories very well.

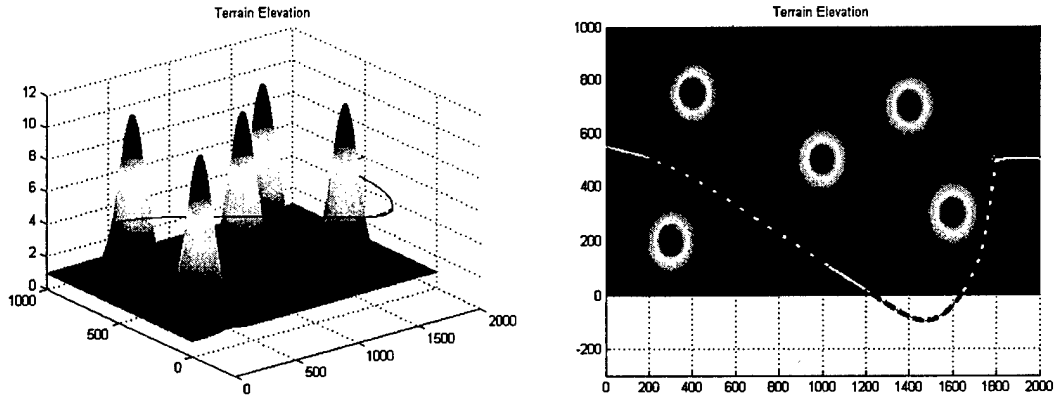

Figure 17: Flight paths from third case. The black line is the commanded path and the blue line is the actual path.

In addition, the program was tested using the simplified formulation described at the beginning of the paper, with the same three terrain maps described above. This was done to compare the results from the two different formulations for these three terrain maps. In all of the cases, the program was unable to find an optimal path that avoided the threats. As described earlier, the optimal path should avoid going over any of the threats. In the first and third cases, with one and five threats, respectively, no solution at all was found. In the second case with three constraints, the only solution involved crossing one of the threats.

3.7 V AS A CONTROL VARIABLE

The code for implementing the velocity as a control variable with the local tangent plane equations of motion was also tested. For this section, the terrain data described above for case 3 was used. In this case, a velocity of 80 feet per second is required in order for the heading rate limit to be reached. Comparatively, a velocity of about 160 feet per second – which is unrealistically high -- is necessary to reach the constraint for the terrain in case 2. The vehicle specifics used for this case are a weight of 5 pounds, a wing span of 2.2 square feet, and a load factor limit of 1.1. The corner velocity for this case is 46.23 feet per second and the maximum velocity is 80 feet per second.

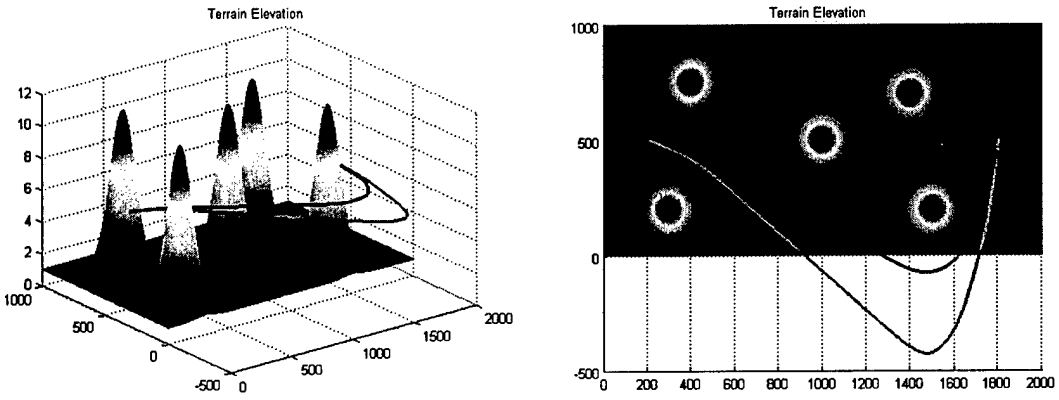

Figure 18: Flight trajectories for the unconstrained path (black line) and the constrained path (purple line).

Figure 18 shows the trajectories from both the unconstrained code and the velocity as a control code. The black line shows the unconstrained path while the constrained path is depicted

in purple. It can be seen in this figure that the constrained path goes much further around the threat than the unconstrained trajectory did. The respective heading rates for these two paths can be seen in Figure 19. The plot on the left shows the heading rate for the unconstrained flight while the plot on the right is the corresponding heading rate for the velocity as a control path. For the portion of the constrained flight when the constraint is hit, the heading rate jumps to a much higher rate. This is due to the fact that the velocity also jumps at that point from the maximum velocity to the corner velocity; this jumps causes the heading rate to jump because they are inversely proportional, as can be seen in equation (76). The velocity for the constrained case can be seen in Figure 20.

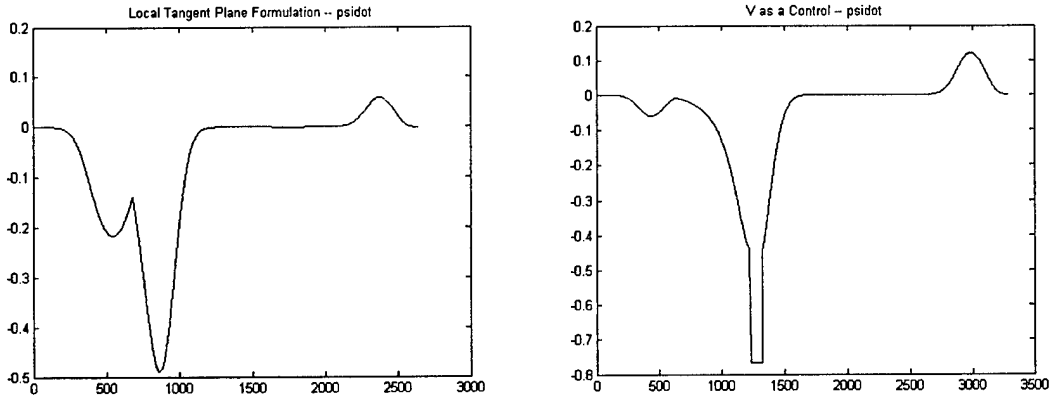

Figure 19: Heading rates for the unconstrained path, on the left, and the constrained path, on the right.

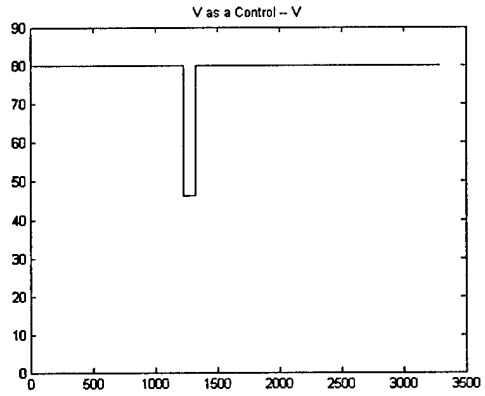

Figure 20:Velocity profile for the velocity as a control trajectory

3.8 POP-UP THREATS

The next task investigated was the case of pop-up threats during flight. In this case, the optimal path is in mid-flight when a stationary threat appears. A new trajectory must then be calculated. To test this, the first results with the Columbus terrain – shown in Figure 7 – were used. However, the constant velocity, local tangent plane formulation was used. In this case, a threat was added to the terrain as a single hill, as shown in Figure 13. In this case, the hill used had a height of 300 feet above the level of the terrain at that point.

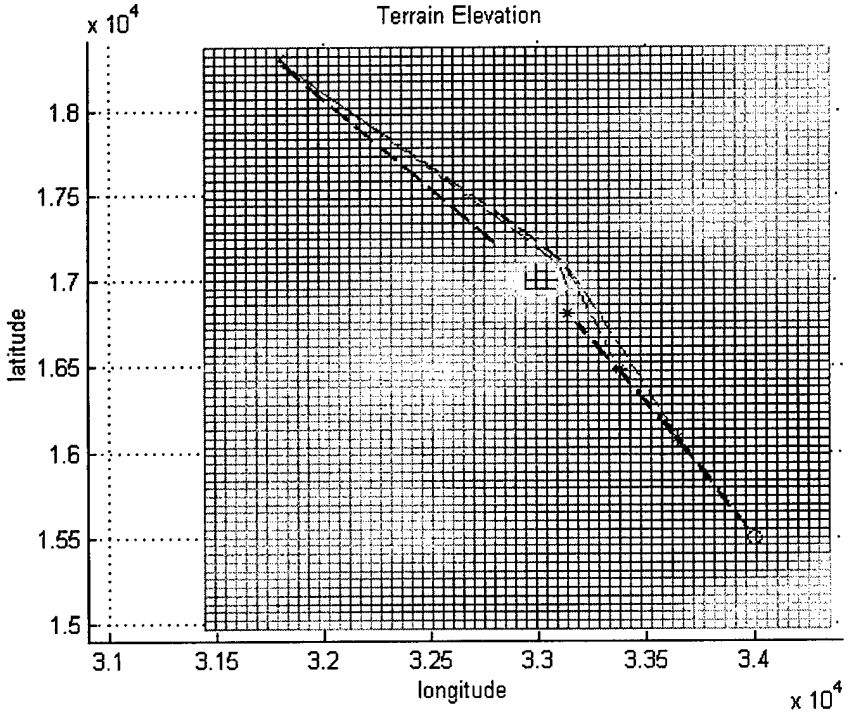

Figure 21: Trajectories found with a pop-up threat.

The results for this section can be seen in Figure 21. In this plot, the black line depicts the original trajectory found; here it goes directly through the new threat. Three different new trajectories are then shown as magenta lines. These depict the results for three different times at which the threat is found; these times are at 17.2 seconds, 29.46 seconds and at 39.79 seconds into the approximately 90 second flight. In each case, this point is marked on the plot with a red star.

4. SUMMARY OF PHASE I PROGRAM RESULTS

The phase I effort focused on demonstrating a robust method for numerical solution of the reduced order problem that is suitable for real-time, on-board implementation. The goal was to embed as much of the full vehicle dynamics as possible in the reduced problem while maintaining a tractable solution process. This was done in steps, starting with the simplest problem formulation of interest, and then adding complexity in small increments. The impact of the added complexity on efficiency of the numerical solution procedure was also evaluated at each step. Those components that cannot be directly accounted for in the reduced solution are to be treated using singular perturbation methods of analysis.

The complete set of Phase I mathematical problem formulations and several solution procedures were given in Chapters 2 and 3. Representative numerical results were also presented, as were results from an initial demonstration of tracking obstacle avoidance trajectories on a rotary wing UAV. These results were first documented in the form of a technical paper presented by the team members at the AIAA Guidance, Navigation and Control conference in August of 2003. However, this report includes many results not available in time for conference paper submission. In this Chapter, we summarize the solution procedures detailed in Chapters 2 and 3 and review their merits and expected limitations.

The effort began with the formulation of the following reduced order problem: find the optimal flight path from point a to point b over complex terrain while taking into account a requirement to avoid static threats and obstacles. The work of P.K. Menon, et. al., in optimal

terrain following and terrain masking flight from the early 1990's was found to be directly relevant, and this approach was adopted as the primary solution process to be investigated.

To begin, we assume the availability of a terrain data base for the region in which flight operations are to be performed. We then process the available data to represent the terrain as a smooth altitude profile as a function of downrange and crossrange coordinates. **We next introduce perturbations in the terrain height to represent threats or obstacles that are to be avoided.** That is, we create fictitious terrain features that are representative of the presence of threat systems, obstacles, no fly zones, or the like. Note that these features can be updated in flight as new information becomes available from on-board sensors or external sources. Note also that the height and shape of the terrain perturbation associated with a particular threat system can be adjusted to reflect properties such as its lethality and the risk of exposure to it, as well as its relative importance in the overall problem formulation. Next the height of the flight path above the terrain is constrained to remain fixed at a specified value (as in nap-of-the-Earth flight operations). A simple performance index is introduced that is the integral of the sum of time and the modified terrain height. A weighting factor is used on each component of the integral to allow the objective to vary from the case of absolute minimum time, to the case of maximum use of terrain masking and/or threat avoidance.

Constant Energy Formulation. We take the indirect approach to set up a solution procedure – applying the 1st order necessary conditions for optimality. In the work of Menon, et. al., flight is constrained to remain tangent to the local terrain at constant velocity. However, in maneuvering flight, it may be undesirable or impossible to maintain constant velocity. A better

approximation during such maneuvers may be that of constant energy, allowing one to trade potential and kinetic energy as needed. The team investigated two solutions to the above problem using the constant energy approximation. In the first, we ignore the vertical component of velocity required to follow the terrain height. The solution can be reduced to the problem of solving three differential equations with only one unknown parameter, the initial aircraft heading. A simple numerical procedure is used to sweep through all possible values of initial heading. This results in a very efficient solution procedure that is well suited to real-time on-board implementation. In the second case, we include the vertical component of velocity required to follow the terrain height. While the costate relations are slightly more complicated, in the end we obtain a solution of the same form; integration of three differential equations and determination of the one unknown parameter, the initial vehicle heading.

Numerical results were generated for both of these cases using simple sinusoidal and then real terrain data. Sample results were included in Chapter 3.

Additional of a Heading Rate Constraint. Practical use of the algorithm will require the ability to enforce a heading rate constraint. When this constraint is not active the solution procedure described above remains unchanged. When the constraint is encountered during flight, no additional unknowns result – all of the initial conditions for the constrained arc are equal to their respective values when the constraint is hit. In the event the solution begins on the constraint boundary, then the simple solution process described above is complicated by the requirement to also determine the initial conditions on three costates.

Constraining Heading Rate through an Angle of Attack Limit. As an alternative to direct constraint of the heading rate, it is possible to constrain it indirectly by imposing a limit on angle of attack. The solution procedure was developed for this case and is summarized in Chapter 2. However, the costate equations are more complicated in this case, and the direct incorporation of the heading constraint is preferred thus far.

Modified Constant Energy Approach. In the work described above, energy is held constant at a nominal value. This results in the flight speed being determined directly from the terrain height. If we climb to a high altitude in the trajectory, the use of the energy state approximation results in the flight speed being determined by the altitude rather than the cruise performance of the aircraft. Thus while the constant energy approximation is quite useful for maneuvering flight, it can lead to inappropriate choices of flight velocity during cruise unless the nominal value of energy is carefully chosen. To overcome this limitation of the constant energy formulation, we introduce an alternate definition for velocity as the linear combination of a nominal value and a perturbation determined by using the constant energy relation operating on a filtered terrain data base. In this formulation the nominal velocity can be set to a standard flight speed, and it will remain near this value (i.e. approximately constant), but will have some fluctuation due to required short term changes in altitude. The filter employed is a high pass filter. Thus low frequency variation in the terrain height is ignored, but steep altitude gradients are still recognized. The choice of filter cutoff frequency determines the blend that occurs between the constant velocity solution and the constant energy approach. Note that the velocity

calculation using the energy state approximation does not use the perturbation in the terrain data base introduced to model threat systems. It only uses the true terrain altitude variation. Numerical results generated with real terrain data were used to compare the modified approach to the constant energy approach. As detailed in Chapters 2 and 3, the resulting trajectories and the associated time of flight are very similar, but the variation in velocity is greatly reduced. The heading rate constraint described above has also been derived for the constant velocity case. This approach was found to provide the benefits of the constant energy approach (i.e. it recognizes the need to trade kinetic and potential energy when the vehicle must climb rapidly to avoid terrain, but does not force the flight velocity to an inappropriate value when climbing or descending in general). Other than introduction of the terrain height filter and the new calculation of velocity, this approach enjoys the same solution procedure as described above (simple sweep of initial heading value).

Employing Velocity as a Control Variable. In all of the work described above, velocity is just a consequence of the other states. We next considered the use of velocity as a control variable, as detailed in later chapters. The optimal solution in this case results in a simple strategy of flying at the velocity limit except when limited in a maneuver by the g-limit. In such case the velocity is limited to respect the g-limit. The relations that must be solved in this case are more complicated, but still tractable. And as in the case when the angle of attack limit is introduced, if the solution starts on the g-limit, one must also solve for the initial conditions on the 3 costates. Since velocity is treated as a control variable in the reduced solution, it is possible

that velocity can be discontinuous. In such case a boundary layer correction is required. However, it is expected that this will rarely be the case when working with real terrain data.

5. ASSESSMENT OF FEASIBILITY

The phase I program was designed to demonstrate the feasibility of developing algorithms appropriate for real-time autonomous air vehicle trajectory optimization using the method of singular perturbations to exploit natural time-scale separation in the vehicle dynamics. In such case, the reduced order problem must only address the translational dynamics, and a boundary layer analysis is used to account for neglected nonlinear aircraft dynamics and to produce an optimal feedback guidance solution. The focus of the phase I effort was development of robust numerical solution procedures for the reduced order problem in the presence of complex 3-D terrain, threats and obstacles.

Excellent results were obtained from the phase I effort. As summarized in the previous Chapter, variations of the reduced order problem have been formulated that embed ever greater amounts of the full problem complexity, and in each case the solution process was reduced by application of the necessary conditions to a simple 1 parameter numerical search. The only exception is when the solution starts on a constraint boundary. In this special case the search must be expanded to include the costate initial conditions. Constraints on turn rate, angle of attack, and g-limits were successfully introduced. C code versions of the algorithms were developed and tested using realistic terrain data, demonstrating practical solution over complex terrain in seconds on a standard desktop PC.

The phase I results clearly establish the feasibility of producing robust numerical solution to the reduced order problem despite the complications of operation in terrain amongst obstacles and threats. The resulting one-parameter search problem can be solved very rapidly with a simple numerical sweep and will support real-time autonomous execution of the optimization algorithm on-board. The simple phase I process by which the step size is adjusted in this one-parameter search is adequate, but can be improved in phase II. It is also possible that one can satisfy all of the necessary conditions to arrive at a solution, but still not have the true optimal solution. Application of the 2nd order necessary conditions may provide additional means to identify the optimal solution in this case, and is to be the subject of investigation in phase II.

The envisioned phase II program will continue the work of phase I to fully develop efficient numerical solution procedures for complex variations of the reduced order problem. In particular the reduced problem formulation should be expanded to include time varying threats, moving terminal conditions, and interior point constraints. Numerical solutions of the full-order optimization problem for candidate mission scenarios could be developed to provide a basis for evaluating the reduction in optimality experienced when employing the reduced solution. This "truth" model could also be used to identify those maneuvers where boundary layer corrections are needed. The boundary layer corrections can then be developed, as well as associated optimal feedback guidance laws. As noted above, the 2nd order necessary conditions should also be explored.

6. RECOMMENDATIONS FOR FURTHER RESEARCH

The specific objectives proposed for a phase II program are presented below.

- Develop a comprehensive set of Phase II mission scenarios that is representative of the sponsor's program interests.

- Extend the Phase I reduced order problem formulation and numerical solution procedure to include:
  - Moving threat systems
  - Moving terminal conditions
  - Interior point constraints
  - Three-dimensional maneuvers with velocity as a control

- Evaluate the ability to track the developed reduced order solution optimal trajectories in high-fidelity nonlinear simulation of six degree-of-freedom high-performance aircraft operating at low altitude over real terrain with realistic simulation of both stationary and moving pop-up threats.

- For a select number of candidate trajectories, construct the full-order optimal trajectory using a multiple shooting algorithm such as BOUNDSCO.

- Compare the full-order and reduced-order optimal trajectories, and quantify the differences. Fly both trajectories with a nominal guidance law in the simulation and again quantify the differences. Identify any flight maneuvers for which construction of a boundary layer solution is expected to be beneficial.

- Perform boundary layer construction for the selected flight phases, if any, where a significant improvement in optimality has been shown to be available.

- Repeat flight simulations of the candidate trajectories using the boundary layer corrections, compare with the full-order optimal solution, and quantify the improvements obtained.

- Further investigate the possibility of conjugate points, and develop a test for the occurrence of these points.

- Evaluate and demonstrate the real-time performance of the developed optimization algorithm in high-fidelity nonlinear simulation for the full range of mission scenarios being investigated.

- Flight demonstrate guided flight of a UAV while employing the real-time path optimization algorithm in at least three challenging mission scenarios by introducing virtual terrain, obstacles and pop-up threats.

REFERENCES

1. Bryson, A. E., Desai, M. N., and Hoffman, W. C., "Energy-State Approximation in Performance Optimization of Supersonic Aircraft," Journal of Aircraft, Vol. 6, No. 6, 1969.

2-3. Bryson, A. E., and Lele, M. L., "Minimum Fuel Lateral Turns at Constant Altitude," AIAA Journal, Vol. 7, No. 6, 1969.

4. Kelly, H. J. "Aircraft Maneuver Optimization by Reduced Order Approximation," in Control and Dynamic Systems, Advances in Theory and Applications, Vol. 10, Academic Press, New York, NY, 1973.

5. Kelley, H. J., and Edelbaum, T. N., "Energy Climbs, Energy Turns, and Asymptotic Expansions," Journal of Aircraft, Vol. 7, No. 1, 1970.

6. Calise, A.J., "Singular Perturbation Methods for Variational Problems in Aircraft Flight," IEEE Trans. on A.C., Vol. AC-21, No. 3, June 1976.

7. Calise, A.J., "Extended Energy Management Methods for Flight Performance Optimization," AIAA Journal, Vol. 15, No. 3, March 1977.

8. Calise, A.J., "A New Boundary Layer Matching Procedure for Singularly Perturbed Systems," IEEE Trans. on A.C., Vol. AC-23, No. 3, June 1978.

9. Calise, A.J., "Singular Perturbation Techniques for On-Line Optimal Flight-Path Control," AIAA J. of Guidance and Control, Vol. 4, No. 4, 1981.

10. Ardema, M. D. "Singular Perturbations in Flight Mechanics," NASA TM X-62, 380, Aug. 1974; Revised July 1977.

11. Naidu, D.S., Calise, A.J., "Singular Perturbations and Time Scales in Guidance and Control of Aerospace Systems: A Survey, AIAA Journal of Guidance, Control, and Dynamics, Vol. 24, No. 6, November-December 2001.

12. Calise, A.J., "Singular Perturbations in Flight Mechanics," in *Applied Mathematics in Aerospace Science and Engineering*, Vol. 44 of Mathematical Concepts and Methods in Science and Engineering, Edited by A. Miele and A. Salvetti, Plenum Press, 1994.

13. Price, D., Calise, A.J., Moerder, D., "Piloted Simulation of an On-Board Trajectory Optimization Algorithm," AIAA J. of Guidance and Control, Vol. 7, No. 3, May 1984.

14. Kim, Eulgon. *Optimal Helicopter Trajectory Planning for Terrain Following Flight.* Thesis. Georgia Institute of Technology. 1990.

15. Menon, P.K., E. Kim, V.H.L. Cheng. "Optimal Trajectory Planning for Terrain Following Flight" Journal of Guidance, Control and Dynamics, Vol. 14, No. 4, July – August 1991, pp. 807 - 813.

16. United States Geological Survey. Terrain Data. ftp://edcftp.cr.usgs.gov/pub/data/DEM/250/

17. Calise, A.J., "Singular Perturbation Techniques for On-Line Optimal Flight-Path Control," AIAA J. of Guidance and Control, Vol. 4, No. 4, 1981.